



# Detection of Virus SARS-CoV-2 Using a Surface Plasmon Resonance Device Based on BiFeO<sub>3</sub>-Graphene Layers

Sofyan A. Taya<sup>1</sup> · Malek G. Daher<sup>1</sup> · Abdulkarem H. M. Almawgani<sup>2</sup> · Ayman Taher Hindi<sup>2</sup> · Samer H. Zyoud<sup>3</sup> · Ilhami Colak<sup>4</sup>

Received: 15 April 2023 / Accepted: 24 April 2023 / Published online: 10 May 2023  
© The Author(s), under exclusive licence to Springer Science+Business Media, LLC, part of Springer Nature 2023

## Abstract

Coronavirus disease (COVID-19) pandemic outbreak is being investigated by severe respiratory syndrome coronavirus-2 (SARS-CoV-2) as a global health issue. It is crucial to propose sensitive and rapid coronavirus detectors. Herein, we propose a biosensor based on surface plasmon resonance (SPRE) for the detection of SARS-CoV-2 virus. To achieve improved sensitivity, a BiFeO<sub>3</sub> layer is inserted between a metal (Ag) thin film and a graphene layer in the proposed SPRE device so that it has the structure BK7 prism/ Ag/ BiFeO<sub>3</sub>/ graphene/ analyte. It has been demonstrated that a small variation in the refractive index of the analyte can cause a considerable shift in the resonance angle caused by the remarkable dielectric properties of the BiFeO<sub>3</sub> layer, which include a high index of refraction and low loss. The proposed device has shown an extremely high sensitivity of 293 deg/RIU by optimizing the thicknesses of Ag, BiFeO<sub>3</sub>, and the number of graphene sheets. The proposed SPRE-based sensor is encouraging for use in various sectors of biosensing because of its high sensitivity.

**Keywords** SARS-CoV-2 · Surface plasmon resonance · BiFeO<sub>3</sub> · Graphene · Sensitivity

## Introduction

A recently discovered human-transmissible virus called coronavirus 2 (SARS-CoV-2) causes severe respiratory syndrome. Globally, hundreds of millions of SARS-CoV-2 positive cases have been found, killing millions of people. The human-transmissible SARS-CoV-2 virus outbreak was announced as a worldwide pandemic by the WHO. The SARS-CoV-2 virus typically consists of a single-stranded RNA and four important proteins: (1) nucleocapsid (N) protein, (2) membrane (M), (3) envelope (E) and (4) spike (S) glycoprotein [1]. The S-glycoprotein can be divided into two types of subunits (S1 and S2), where S1 binds

with the host cell receptor human angiotensin-converting enzyme 2 (ACE2) and S2 is liable for membrane fusion [2]. The human heart, kidneys, lungs, and other organs all contain ACE2, which enables the viral spike protein to enter cells [1]. The brain, lungs, heart, and kidneys experience significant damage as a result of the viral spike protein's activation [3]. As a result, clinical research on the development of vaccines and detection methods to stop the spread of the infectious disease must focus on neutralizing the SARS-CoV-2 virus spike protein. In clinical studies, dozens of vaccines have been developed to neutralize the SARS-CoV-2 viral spike's receptor-binding domain [4]. More than 90% of SARS-CoV-2 vaccinations are effective against the virus [4, 5]. COVAX has been trying to accelerate the creation of SARS-CoV-2 vaccines, their commercial production, and their fair distribution [4]. However, SARS-CoV-2 viruses are expanding very rapidly. Novel variants of coronavirus have been discovered with altered mutations [6]. Early identification is essential for controlling the pandemic since the vaccine is not commercially available everywhere due to economic situations. To effectively monitor infected individuals for successful quarantine and prompt treatment, it is crucial to have extremely sensitive, quick-test findings, and affordable analytical techniques. The SARS-CoV-2 virus is currently detected using the real-time

✉ Sofyan A. Taya  
staya@iugaza.edu.ps

<sup>1</sup> Physics Department, Islamic University of Gaza, P.O. Box 108, Gaza, Palestine  
<sup>2</sup> Electrical Engineering Department, College of Engineering, Najran University, Najran, Kingdom of Saudi Arabia  
<sup>3</sup> Department of Mathematics and Sciences, Ajman University, Ajman, United Arab Emirates  
<sup>4</sup> Department of Electrical and Electronics Engineering, Nisantasi University, Istanbul, Turkey

reverse-transcriptase-polymerase chain reaction (RTPCR) technology as a standard reference. Results from the RTPCR method are obtained in 1–3 days [7]. The lengthy extraction of virus ribonucleic acid (RNA) has an impact on the accuracy of detection. Zhao et al. developed a pcMNPs methodology for virus RNA extraction [8] to overcome the lengthy RNA extraction process. The sensitivity of the RTPCR technique varies between 45 and 60% for RNA extraction whereas employing pcMNPs increases the sensitivity to about 92% [7]. The COVID-19 IgG/IgM fast test kit is utilized in clinical settings to identify antibodies (IgG/IgM), with IgG becoming detectable in an affected patient blood after 3–6 days and IgM becoming detectable after 8 days [9, 10]. Although less sensitive than the RTPCR method, the SARS-CoV-2 antigen fast test kit is still applied to identify the COVID-19 virus [11, 12]. Moreover, the chest computed tomography (CT) scan is checked to corroborate the test results. If the fast test kit is not handled properly, it produces false findings [13].

Surface plasmon sensors (SPREs)-based biosensors have been proposed for future COVID-19 viral detections [14–18]. Generally, SPRE-based sensors are characterized by rapid detection, accuracy and high sensitivity [19–22].

For the past three decades, SPRE has been a widely used method to identify biomolecular interactions for clinical applications [23]. Several SPRE-based sensors have been employed in biosensing applications, including localized and compact SPRE biosensors [24]. There is no essential difference in the principle of operation of SPRE-based biosensors. Depending on light coupling, the SPRE structures can be classified into four sets: grating-based, fiber optic-based, waveguide-based and prism-based. Researchers preferred prism-based SPRE structure due to its accurate realization [25]. There are two possible setups for the prism-based SPRE sensor: (1) Kretschmann and (2) Otto. Kretschmann configuration is preferred for experimental work with superior results using the angular interrogation method due to less absorption loss [26, 27]. The stimulation of the surface plasmons (SPNs) can be applied to the SPRE sensors for producing the surface plasmon waves (SPWEs) on the metallic film by applying the attenuated total reflection method [28]. The SPWEs oppose the light energy of the plasmons, and that light energy is translated as reflected light in the total internal reflection principle. At the metal-dielectric contact, the SPWEs transpire the evanescent wave (EWE) whose intensity exponentially decays in the direction perpendicular to the interface. The resonance oscillation of the SPWEs is called the SPRE phenomenon which shows the minimum reflectivity. The reflectance profile depends on the surface refractive index (RIX). The resonance dip of the reflected radiation varies depending on any variations in the RIX of the materials utilized in the construction of the SPRE biosensor. The standard SPRE sensors achieve broader SPRE curves and less resonance angle change. The ultimate goal of

researchers is to establish sharp curves and higher resonance angle changes to improve the sensor performance [29]. As a result, many researchers have inserted dielectric layers over the metal layer to enhance SPRE performance and provide protection for the metal film from oxidation [30]. Due to its enormous potential, high electric field absorption, and tiny gap, BiFeO<sub>3</sub> is a promising material that has received a lot of attention [31]. Although the SPRE performance can be enhanced by using dielectric materials, it is difficult to maintain its optical properties and complex geometry. In order to mitigate this issue, researchers have proposed hybrid structures incorporating bimolecular recognizing elements (BRETs), which can provide a high SPRE performance [32]. Though, SPRE biosensors with good performance are still lacking. Several interesting two-dimensional (2D) transition metal dichalcogenides (TMDEs) materials are available to fulfill this challenge. Due to its unique optical and electrical properties, the graphene family has attracted a lot of attention recently [33, 34]. In recent work, graphene-MoS<sub>2</sub> layers have been used to design a biosensor for biomolecule detection. The sensitivity was observed to enhance when an additional nanolayer of silicon is used [35–40].

Despite the fact that several SPRE biosensors have already been developed by other researchers, further research is still necessary to enhance the performance characteristics and advance the development of sensors.

The novelty of the current work lies in the fact that SPRE-based sensors are characterized by rapid detection, accuracy and high sensitivity. So far, very few articles have been published on using SPRE-based sensors for the detection of SARS-CoV-2 virus. The current paper proposes an efficient structure based on SPRE for the detection of this dangerous virus that can cause severe respiratory syndrome.

This work reports a novel SPRE sensor that can efficiently detect SARS-CoV-2 virus. The hybrid structure comprises a BK7 prism, Ag, BiFeO<sub>3</sub>, graphene and sensing medium. The performance of the SPRE biosensor is evaluated in terms of the full-width at half maximum (FWHM), detection accuracy, sensitivity and figure of merit. At a wavelength of 633 nm, the sensor performance is numerically examined. The current paper is structured as follows. The theoretical and numerical modeling of the suggested SPRE biosensor is explained in section "Structure Considerations". Section "Results and Discussion" reports the results obtained and the discussion. The present study is finally concluded in section "Conclusion".

## Structure Considerations

### Model Design

A biosensor based on SPRE is proposed (Fig. 1). It has five layers: BK7 prism, Ag, BiFeO<sub>3</sub>, graphene, and analyte layer.

The thicknesses and RIXs of the silver layer, BiFeO<sub>3</sub>, and graphene are denoted as  $d_{Ag}$ ,  $d_{BF}$  and  $d_G$  and  $n_{Ag}$ ,  $n_{BF}$  and  $n_G$ , respectively.

The RIX of BK7 prism is given by [41]

$$n_p(\lambda) = \sqrt{1 + \frac{1.03961212\lambda^2}{\lambda^2 - 0.00600069867} + \frac{1.01046945\lambda^2}{\lambda^2 - 103.560653} + \frac{0.231792344\lambda^2}{\lambda^2 - 0.0200179144}} \quad (1)$$

The Ag RIX is obtained as (Drude-Lorentz model) [42]

$$n_{Ag}(\lambda) = 1 - \frac{\lambda_c \lambda^2}{\lambda_p^2 (\lambda_c + i\lambda)} \quad (2)$$

with  $\lambda_p = 0.1454 \mu\text{m}$  and  $\lambda_c = 0.1761 \mu\text{m}$  are the plasma and collision wavelengths of the Ag material. The RIX of BiFeO<sub>3</sub> is 2.9680.

The graphene RIX is given by [43]

$$n_G(\lambda) = 3 + \lambda \frac{C}{3} i, C = 5.446 \mu\text{m}^{-1} \quad (3)$$

Concerning the sensing medium, phosphate-buffered solution (PBSN) may be utilized as a RIX of PBSN that is deliberated as  $ns = 1.334 + \Delta ns$ , where  $\Delta ns$  is the index variation as a result of analyte-ligand interaction on the sensor surface. According to earlier research [44], a PBSN buffer containing SARS-CoV-2 glycoprotein may dissolve HEPES

10 mM and 120 mM NaCl solution, and the RIX of PBSN can be experimentally measured.

When used, various quantities of HEPES solution were added to a 120 mM NaCl solution and a good linear relation between the RIX of PBSN and HEPES concentration ranging from 0 to 20 mM was found, and this relationship can be expressed as [44]

$$n = 0.00004y + 1.334 \quad (4)$$

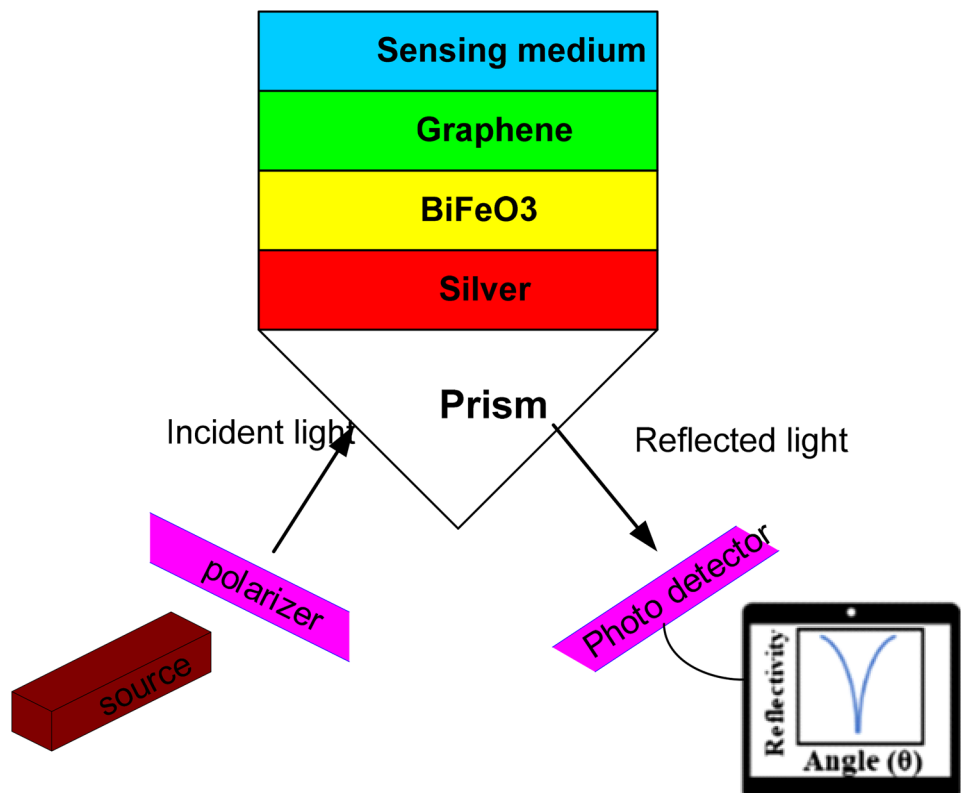
where  $n$  is the RIX index of PBSN.  $y$  is the solution of HEPES (mM). In this investigation, diverse concentrations of HEPES solution have been given in 10 mM, so the RIX of the sensing medium was assumed to be 1.3344 [45].

### Mathematical Modeling

Along the  $z$ -axis, all layers are organized into a stack. The dielectric constant and thickness for each layer are  $\epsilon_k$  and  $d_k$ . The relationship between the tangential fields of the first boundary at  $z = 0$  and those of the final boundary at  $z = z_{N-1}$  is given by the characteristic matrix ( $W$ ) as

$$\begin{bmatrix} F_1 \\ G_1 \end{bmatrix} = W \begin{bmatrix} F_{N-1} \\ G_{N-1} \end{bmatrix} \quad (5)$$

**Fig. 1** SPRE device based on BiFeO<sub>3</sub>-graphene layers.



where  $F_i$  and  $G_i$  are the electric and magnetic fields at the  $i$  boundary. The characteristic matrix ( $W_j$ ) of the  $j^{\text{th}}$  layer can be written as

$$W_j = \begin{bmatrix} \cos(\beta_j) & -\frac{i \sin(\beta_j)}{Y_j} \\ -i Y_j \sin(\beta_j) & \cos(\beta_j) \end{bmatrix} \quad (6)$$

$\beta_j$  is the phase variation which can be written as

$$\beta_j = \frac{2\pi}{\lambda} d_j (\epsilon_j - (n_1 \sin \theta_1)^2)^{0.5} \quad (7)$$

where  $n_j$  is the RIX,  $\epsilon_j$  is the dielectric permittivity, and  $d_j$  is the thickness.  $\theta_1$  and  $n_1$  are the prism angle of incidence and RIX.

For TM wave  $Y_j = (\epsilon_j - (n_1 \sin \theta_1)^2)^{0.5} / \epsilon_j$ .

$W_T$  is the characteristic matrix of the device shown in Fig. 1 which can be expressed as

$$W_T = W_{Ag} W_{BF} W_G = \begin{bmatrix} W_{11} & W_{12} \\ W_{21} & W_{22} \end{bmatrix} \quad (8)$$

where  $W_{ij}$  are the elements of the matrix.

The reflection coefficient ( $r$ ) for the TM wave

$$r = \frac{(W_{11} + W_{12} Y_N) Y_1 - (W_{21} + W_{22} Y_N)}{(W_{11} + W_{12} Y_N) Y_1 + (W_{21} + W_{22} Y_N)} \quad (9)$$

The reflection intensity can be written as

$$R = |r|^2 \quad (10)$$

SPRE sensor performance can be measured by means of sensitivity ( $S$ ) and figure of merit ( $FoM$ ). A modification of resonance angle,  $\Delta\theta_{\text{res}}$ , takes place as a result of the change in the analyte RI,  $\Delta n_s$ . The sensitivity can be defined in terms of  $\Delta\theta_{\text{res}}$  and  $\Delta n_s$  as

$$S = \frac{\Delta\theta_{\text{res}}}{\Delta n_s} \quad (11)$$

The  $FWHM$  of the dip is given by

$$FWHM = \theta_2 - \theta_1 \quad (12)$$

where  $\theta_1$  and  $\theta_2$  are the resonant angles at 50% intensity.

The detection accuracy ( $DA$ ) of the SPRE sensor can be obtained by using

$$DA = \frac{1}{FWHM} \quad (13)$$

The  $FoM$  depends on both  $S$  and  $DA$

$$FOM = S \times DA \quad (14)$$

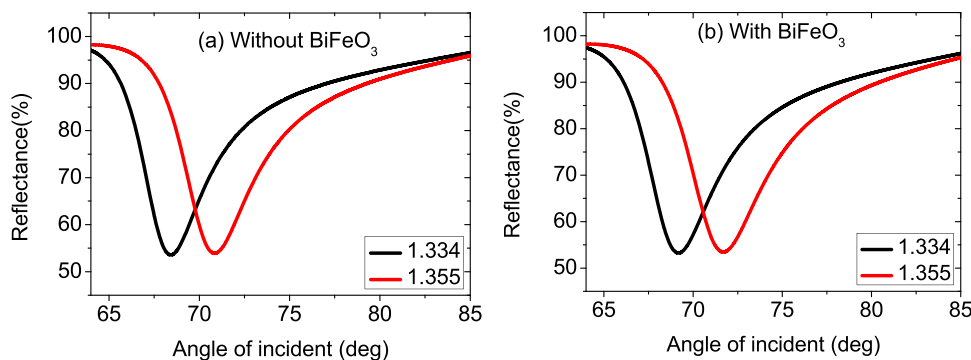
## Results and Discussion

Here, we present a Kretschmann-design SPRE biosensor, which includes a prism to give the SPNs the required momentum. BK7 prism is used in this work because of its low RI. Applying TM light ( $\lambda = 633$  nm), SPN coupling is realized at the contact between the metal and dielectric. A reflectance change is observed due to the variation in the analyte RIX. The reflectance curve exhibits a sharp dip at resonance conditions. This indicates that maximum energy is transferred to the SPNs at resonance conditions. The refractive indices of the materials used are  $n_p = 1.5151$ ,  $n_{Ag} = 0.0562 + 4.2776i$ ,  $n_{BF} = 2.9680$  and  $n_G = 3 + 1.149106i$ .  $n_p$ ,  $n_{Ag}$ , and  $n_G$  are calculated using Eqs. (1), (2) and (3), respectively, at  $\lambda = 633$  nm. The thicknesses of the layers are initially considered as  $d_{Ag} = 30$  nm,  $d_{BF} = 1$  nm and  $d_G = M \times 0.34$  nm ( $M = 1$ ). Five different concentrations of 0, 150, 275, 400, and 525 mM mixing in the buffer channel are considered. According to Eq. (4), the analyte RIX ranges from 1.334 to 1.355. Wolfram Mathematica 11.2 software has been used to conduct numerical simulations.

Figure 2 shows the reflectance profile for various device arrangements. The findings imply that the resonant angle shifts toward a larger value in response to the increase in the sensing medium RIX. The resonance curve for a traditional SPRE sensor using Ag-Graphene layers is shown in Figure 2a. The sensitivity Eq. (11) found for the SPRE sensor (without BiFeO<sub>3</sub>) is 114.29 deg/RIU.  $DA$  and  $FoM$  Eqs. (13) and (14) obtained from the resonance curve are  $191.9 \times 10^{-3} \text{ deg}^{-1}$  and  $21.93 \text{ RIU}^{-1}$ , respectively. After introducing a 1 nm BiFeO<sub>3</sub> layer in the conventional SPRE sensor, the sensitivity becomes 120.95 deg/RIU as illustrated in Fig. 2b which means an improvement of 5.83%. In this case,  $DA$  and  $FoM$  achieved with the BiFeO<sub>3</sub> layer are  $181.4 \times 10^{-3} \text{ deg}^{-1}$  and  $21.94 \text{ RIU}^{-1}$ , respectively. Thus, the device with the structure BK7 prism/Ag/ BiFeO<sub>3</sub> /graphene/ sensing medium will be used in the next parts of the paper due to its better performance.

The impacts of certain factors on the sensitivity of the SPRE sensor are examined. These factors include the number of graphene layers, BiFeO<sub>3</sub> layer thickness, metal layer thickness, and the RIX of the sensing medium. As illustrated in Fig. 3a, various thicknesses of Ag (between 30 and 60 nm) are employed. The calculated sensitivities for silver layer thicknesses of 30, 40, 50, and 60 nm, respectively, are 120.95, 126.67, 131.4, and 134.29 deg/RIU. For Ag-layer thicknesses  $> 60$  nm, no dip can be observed in the reflectance curve. Therefore, the optimum thickness of the Ag layer is 60 nm which will be considered in the next investigation. The BiFeO<sub>3</sub> layer thickness is varied between

**Fig. 2** Reflectance profile of the proposed SPRE sensor. **a** without BiFeO<sub>3</sub> and **b** with a BiFeO<sub>3</sub> layer



1 and 7 nm and the sensitivity is calculated for each thickness (Fig. 3b). The sensitivities are found as 134.29, 152.38, 189.52 and 282.86 deg/RIU for  $d_{BF} = 1, 3, 5$  and 7 nm. For  $d_{BF} > 7$  nm, the resonant dip disappears. Hence, the optimum BiFeO<sub>3</sub> layer thickness is  $d_{BF} = 7$  nm. A graphene sheet has a thickness of 0.34 nm. The graphene layer is assumed to have a number of  $M$  sheets. The reflectance profile is investigated for different  $M$  and the sensitivity is calculated and found as 282.86, 293.81, 275.2 and 228.57 deg/RIU for  $M = 1, 2, 3$  and 4, respectively as shown in Fig. 3c. Therefore, the optimum number of graphene sheets is  $M = 2$ . Figure 3d shows the sensitivity as a function of the chemical potential ( $\mu_C$ ) of graphene. The graphene permittivity ( $\epsilon_G$ ) can be written as

$$\epsilon_G = 1 + \frac{i \sigma_G}{\omega \epsilon_0 d_G} \tag{13}$$

where  $\sigma_G$  is the graphene surface conductivity which is given by

$$\sigma_G = \frac{e^2}{\pi h^2} \frac{k_B T}{\Gamma_G - i\omega} \left[ \frac{\mu_C}{k_B T} + 2 \ln \left( e^{\frac{-\mu_C}{k_B T}} + 1 \right) \right] \tag{14}$$

where  $k_B, T, \Gamma_G$  and  $\mu_C$  are Boltzmann constant, temperature, graphene phenomenological scattering rate, and chemical potential. The graphene RIX is related to  $\epsilon_G$  through the relation  $n_G = \sqrt{\epsilon_G}$ . The chemical potential of graphene is varied and the sensitivity is calculated. Figure 3d shows the sensitivity of the proposed structure versus the chemical

**Fig. 3** Sensitivity optimization. **a** Sensitivity versus the thickness of silver at  $d_{BT} = 1$  nm and  $M = 1$ . **b** Sensitivity versus the thickness of BiFeO<sub>3</sub> at  $d_{Ag} = 60$  nm and  $M = 1$ . **c** Sensitivity versus the number of graphene sheets at  $d_{Ag} = 60$  nm and  $d_{BF} = 7$  nm. **d** Sensitivity versus the chemical potential of graphene at  $d_{Ag} = 60$  nm,  $d_{BF} = 7$  nm and  $M = 2$

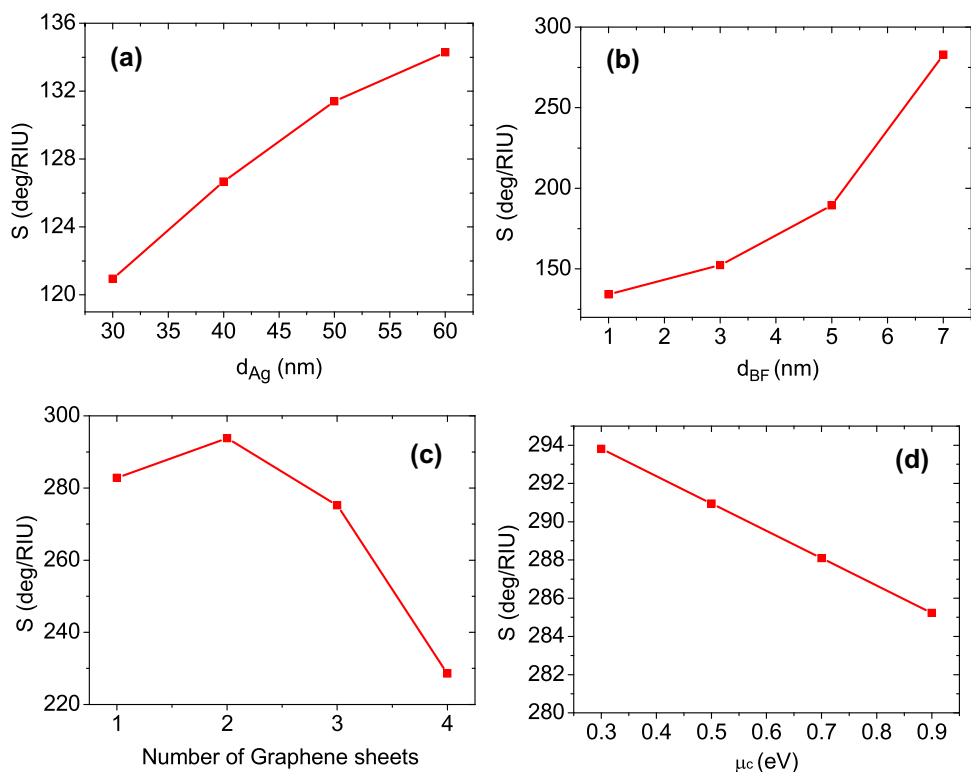
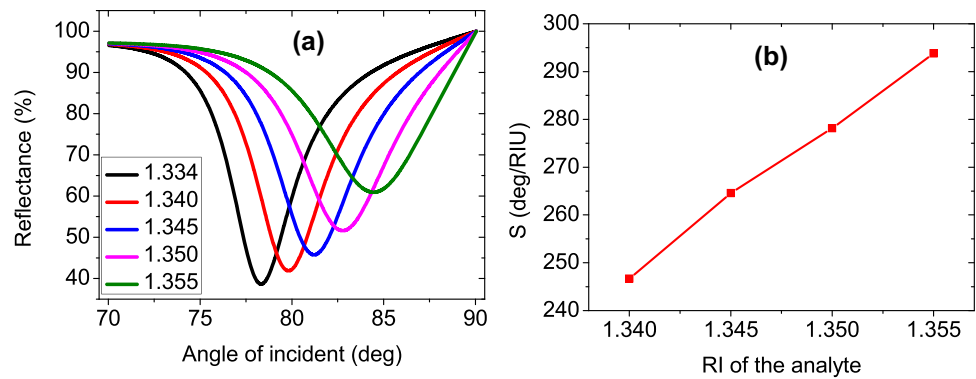


**Fig. 4** **a** Reflectance curve of the proposed SPRE sensors for different concentrations. **b** Sensitivity versus the analyte RIX for the proposed SPRE structure



potential of graphene. The sensitivity decreases slightly as the chemical potential of graphene increases. The highest sensitivity of 293.81 is attained when  $\mu_C = 0.3$  eV.

Figure 4a displays the resonant dips of the reflectance curve for various SARS-CoV-2 solution concentrations. The parameters are set as  $d_{Ag} = 60$  nm,  $d_{BF} = 7$  nm, and  $d_G = M \times 0.34$  nm ( $M = 2$ ) as optimum values. The resonant angle is observed at  $78.34^\circ$  when 0.0 mM is used as the sensing medium. It is noted that as SARS-CoV-2 concentration in the sensing medium solution is increased, the resonant dip moves to higher resonant angles. Resonant angles are found at  $79.82^\circ$ ,  $81.25^\circ$ ,  $82.79^\circ$  and  $84.51^\circ$  for concentrations of 150, 275, 400 and 525 mM, respectively. We have used the reflectance profile to calculate the sensitivity of the sensor to the sensing medium. The sensitivities are found as 246.67, 264.55, 278.12 and 293.81 deg/RIU for the samples having concentrations of 150, 275, 400 and 525 mM, respectively,

as shown in Fig. 4b. SARS-CoV-2 concentrations, analyte RI, dip position, angular shift and sensitivity are presented in Table 1. The highest sensitivity of the biosensor is 293.81 deg/RIU for a concentration of 525 mM, which is an ultra-high value as compared to the recently published papers as shown in Table 2.

Finally, the fabrication techniques of the proposed sensor have to be illustrated. A thin layer of 60 nm of Ag metal has to be deposited on the BK7 prism. The most common deposition methods include ion plating evaporation, laser beam evaporation, vacuum thermal evaporation, and electron beam evaporation. A 7 nm layer of BiFeO<sub>3</sub> has to be grown on the Ag film. The deposition of BiFeO<sub>3</sub> thin film can be achieved using pulsed laser deposition. Two layers of graphene are then deposited on the top of the BiFeO<sub>3</sub> thin film. Chemical vapor deposition can be used for graphene deposition.

**Table 1** Variation of the sensitivity with SARS-CoV-2 solution concentration

SARS-CoV-2 solution concentration (mM)	RI	Dip position (deg)	Angle shift (deg)	S (deg/RIU)
0.0	1.334	78.34	-	-
150	1.340	79.82	1.48	246.67
275	1.345	81.25	2.91	264.55
400	1.350	82.79	4.45	278.12
525	1.355	84.51	6.17	293.81

**Table 2** Comparing the current work with the most recently published SPRE biosensors

Techniques	Year	Sensitivity (deg/RIU)	Reference
Graphene-based SPRE biosensor modeling	2019	121.67	[46]
MXene and black phosphorus-based SPRE biosensor	2019	190.22	[47]
SPRE sensor for DNA hybridization	2020	156.33	[45]
SPRE sensor employing a very thin plasma layer	2021	103	[19]
SPRE sensor having MoS <sub>2</sub> and graphene layers.	2021	194.12	[48]
SPRE biosensor having BiFeO <sub>3</sub> and graphene layers.	2022	293.81	Current work

## Conclusion

In this work, SPRE-based biosensor has been theoretically designed and investigated for the detection of SARS-CoV-2 virus. The proposed structure has been explored by employing the conventional technique of TMM. The structure is examined without and with the BiFeO<sub>3</sub> layer. It is found that the presence of a 1 nm BiFeO<sub>3</sub> layer can improve the sensitivity by 5.83%. The sensitivity is then examined with the Ag and BiFeO<sub>3</sub> layer thicknesses. It is found that the optimum values of Ag and BiFeO<sub>3</sub> layers that correspond to the maximum sensitivity are 60 nm and 7 nm, respectively. The optimum number of graphene sheets is 2. The variation of the sensitivity is studied with the SARS-Cov-2 concentration. The highest sensitivity is found as 293 deg/RIU corresponding to a SARS-Cov-2 concentration of 525 mM (RIX of a sensing medium of 1.355). It is believed that the proposed device can open a new window for the efficient detection of SARS-CoV-2.

**Acknowledgement** The authors are thankful to the Deanship of Scientific Research at Najran University for funding this work under the Research Groups Funding program grant code (NU/RG/SERC/12/4).

**Author Contribution** The authors confirm their contribution to the paper as follows: study conception and design (Sofyan A. Taya and Malek G. Daher). Software (Abdulkarem H. M. Almawgani). Interpretation of results (Malek G. Daher and Ilhami Colak). Draft manuscript preparation (Ayman Taher Hindi and Malek G. Daher). Writing the final version (Samer H. Zyoud, Sofyan A. Taya). Supervision (Sofyan A. Taya). All authors reviewed the results and approved the final version of the manuscript.

**Availability of Data and Material** Detail about data has been provided in the article.

**Code Availability** The used code can be obtained from the corresponding author upon request.

## Declarations

**Ethics Approval** This study does not require ethics approval.

**Consent to Participate** No consent to participate is required for this study.

**Consent for Publication** No consent for publication is required for this study.

**Conflicts of Interest** The authors declare no conflict of interest.

## References

- Astuti I (2020) Ysrafil severe acute respiratory syndrome coronavirus 2 (SARS-CoV-2): An overview of viral structure and host response. *Diabetes Metab Syndr* 14:407–412
- Wong SK, Li W, Moore MJ, Choe H, Farzan M (2004) A 193-amino acid fragment of the SARS coronavirus S protein efficiently binds angiotensin-converting enzyme 2. *J Biol Chem* 279:3197–3201
- Gheblawi M, Wang K, Viveiros A, Nguyen Q, Zhong J-C, Turner AJ, Raizada MK, Grant MB, Oudit GY (2020) Angiotensin converting enzyme 2: SARS-CoV-2 receptor and regulator of the renin-angiotensin system. *Circ. Res.* 126:1456–1474
- Knoll MD, Wonodi C (2021) Oxford–AstraZeneca COVID-19 vaccine efficacy. *Lancet* 397:72–74
- Voysey M, Clemens SAC, Madhi SA, Weckx LY, Folegatti PM, Aley PK, Angus B, Baillie VL, Barnabas SL, Bhorat QE et al (2021) Safety and efficacy of the ChAdOx1 nCoV-19 vaccine (AZD1222) against SARS-CoV-2: An interim analysis of four randomised controlled trials in Brazil, South Africa, and the UK. *Lancet* 397:99–111
- Wise J (2020) Covid-19: New coronavirus variant is identified in UK. *BMJ* 371:m4857
- Cui F, Zhou HS (2020) Diagnostic methods and potential portable biosensors for coronavirus disease 2019. *Biosens Bioelectron* 165:112349
- Zhao Z, Cui H, Song W, Ru X, Zhou W, Yu X (2020) A simple magnetic nanoparticles-based viral RNA extraction method for efficient detection of SARS-CoV-2. *bioRxiv*
- Hou H, Wang T, Zhang B, Luo Y, Mao L, Wang F, Wu S, Sun Z (2020) Detection of IgM and IgG antibodies in patients with coronavirus disease 2019. *Clin Transl Immunol* 9:e01136
- Akib TBA, Mou SF, Rahman MM, Rana MM, Islam MR, Mehedi IM, Mahmud MAP, Kouzani AZ (2021) Design and numerical analysis of a graphene-coated SPR biosensor for rapid detection of the novel coronavirus. *Sensors* 21:3491. <https://doi.org/10.3390/s21103491>
- Mak GC, Cheng PK, Lau SS, Wong KK, Lau CS, Lam ET, Chan RCW, Tsang DNC (2020) Evaluation of rapid antigen test for detection of SARS-CoV-2 virus. *J Clin Virol* 129:104500
- Krüttgen A, Cornelissen CG, Dreher M, Hornef MW, Imöhl M, Kleines M (2021) Comparison of the SARS-CoV-2 Rapid antigen test to the real star Sars-CoV-2 RT PCR kit. *J Virol Methods* 288:114024
- Korevaar DA, Kootte RS, Smits LP, Aardweg JGVD, Bonta PI, Schinkel J, Vigeveno RM, Berk IAVD, Scheerder MJ, Lemkes BA et al (2020) Added value of chest computed tomography in suspected COVID-19: An analysis of 239 patients. *Eur Respir J* 56:2001377
- Qiu G, Gai Z, Tao Y, Schmitt J, Kullak-Ublick GA, Wang J (2020) Dual-functional plasmonic photothermal biosensors for highly accurate severe acute respiratory syndrome coronavirus 2 detection. *ACS Nano* 14:5268–5277
- Shrivastav AM, Cvelbar U, Abdulhalim I (2021) A comprehensive review on plasmonic-based biosensors used in viral diagnostics. *Commun Biol* 4:1–12
- Samson R, Navale GR, Dharne MS (2020) Biosensors: Frontiers in rapid detection of COVID-19. *3 Biotech* 10:1–9
- Taha BA, Al Mashhadany Y, Hafiz Mokhtar MH, Dzulkefly Bin Zan MS, Arsad N (2020) An analysis review of detection coronavirus disease 2019 (COVID-19) based on biosensor application. *Sensors* 20:6764
- Hossain B, Islam M, Abdulrazak LF, Rana M, Akib TBA, Hassan M (2019) Graphene-coated optical fiber SPR biosensor for BRCA1 and BRCA2 breast cancer biomarker detection: a numerical design-based analysis. *Photon Sens.* 10:67–79
- Taya SA, Al-Ashi NE, Ramahi OM, Colak I, Amiri IS (2021) Surface plasmon resonance-based optical sensor using a thin layer of plasma. *J Opt Soc Am B* 28:2362–2337. <https://doi.org/10.1364/JOSAB.420129>
- Kullab Hani M, Taya Sofyan A, El-Agez Taher M (2012) "Metal-clad waveguide sensor using a left-handed material as a core layer. *J Opt Soc Am B* 29(5):959–964. <https://doi.org/10.1364/JOSAB.29.000959>
- Kullab Hani M, Taya Sofyan A (2013) Peak type metal-clad waveguide sensor using negative index materials. *Int J Electron*

- Commun (AEÜ) 67(11):984–986. <https://doi.org/10.1016/j.aeue.2013.05.012>
22. Kullab Hani M, Taya Sofyan A (2014) Transverse magnetic peak type metal-clad optical waveguide sensor. *Optik - Int J Light Electron Opt* 125(1):97–100. <https://doi.org/10.1016/j.ijleo.2013.06.092>
  23. Fen YW, Yunus WMM, Talib ZA (2012) Real-time monitoring of lead ion interaction on gold/chitosan surface using surface plasmon resonance spectroscopy. *Indian J Phys* 86:619–623. <https://doi.org/10.1007/s12648-012-0082-6>
  24. Peng W, Liu Y, Fang P, Liu X, Gong Z, Wang H, Cheng F (2014) Compact surface plasmon resonance imaging sensing system based on general optoelectronic components. *Opt Express* 22:6174–6185
  25. Jabbari S, Dabirmanesh B, Arab SS, Amanlou M, Daneshjou S, Gholami S, Khajeh K (2016) A novel enzyme based SPR biosensor to detect bromocriptine as an ergoline derivative drug. *Sens Act B Chem* 240:519–527. <https://doi.org/10.3390/sens11020043>
  26. Vasimalla Y, Pradhan HS (2021) A highly performed SPR biosensor based on bismuth ferrite-bromide materials-BP/graphene hybrid structure. *Opt Quant Electron* 53:695. <https://doi.org/10.1007/s11082-021-03347-3>
  27. Lee KL, Lee CW, Wang WS, Wei PK (2007) Sensitive biosensor array using surface plasmon resonance on metallic nanoslits. *J Biomed Opt* 12(4):044023. <https://doi.org/10.1117/1.2772296>
  28. Yesudasu V, Pradhan HS, Pandya RJ (2021) Recent progress in surface plasmon resonance based sensors: a comprehensive review. *Helv* 7(3):e06321. <https://doi.org/10.1016/j.heliy>
  29. Kravets VG, Jalil R, Kim YJ, Ansell D, Aznakayeva DE, Thackray B, Belle BD, Withers F, Radko IP, Han Z, Bozhevolnyi SI, Novoselov KS, Geim AK, Grigorenko AN (2014) Graphene protected copper and silver plasmonics. *Sci Rep*. <https://doi.org/10.1038/srep05517>
  30. Shalabney A, Abdulhalim I (2010) Electromagnetic fields distribution in multilayer thin film structures and the origin of sensitivity enhancement in surface plasmon resonance sensors. *Sens Act A Phys* 159(1):24–32. <https://doi.org/10.1016/j.sna.2010.02.005>
  31. Papich MG (2016) Kanamycin Sulfatein: Saunders Handbook of Veterinary Drug. Elsevier, London
  32. Neto AHC, Guinea F, Peres NMR, Novoselov KS, Geim AK (2009) The electronic properties of graphene. *Rev Mod Phys* 81(1):109–162. <https://doi.org/10.1103/RevModPhys.81.109>
  33. Wu L, Guo J, Wang Q, Lu S, Dai X, Xiang Y, Fan D (2017) Sensitivity enhancement by using few-layer black phosphorus-graphene/TMDCs heterostructure in surface plasmon resonance biochemical sensor. *Sens Actuators B Chem* 249:542–548. <https://doi.org/10.1016/j.snb.2017.04.110>
  34. El-Amassi Dena M, Taya Sofyan A (2017) Reflection through a parallel-plate waveguide formed by two graphene sheets. *Photonics Nanostruct Fundamentals Appl* 24:53–57. <https://doi.org/10.1016/j.photonics.2017.03.008>
  35. Zohre S, Soroosh M, Farmani A (2023) Design and numerical simulation of a sensitive plasmonic-based nanosensor utilizing MoS<sub>2</sub> monolayer and graphene. *Diam Relat Mater* 131:109594
  36. Zangeneh AM, Farmani A, Mozaffari MH, Mir A (2022) Enhanced sensing of terahertz surface plasmon polaritons in graphene/J-aggregate coupler using FDTD method. 125:109005. <https://doi.org/10.1016/j.diamond.2022.109005>
  37. Farmani Ali, Mir Ali (2019) Graphene sensor based on surface plasmon resonance for optical scanning. *IEEE Photonics Technol Lett* 31(8):643–646. <https://doi.org/10.1109/LPT.2019.2904618>
  38. Zanganeh AM, Farmani A, Mozaffari MH, Mir A (2022) Design optimization and fabrication of graphene/J-aggregate kretschmann-raether devices for refractive index sensing using plasmon-induced transparency phenomena. *Plasmonics* 17:811–821. <https://doi.org/10.1007/s11468-021-01591-7>
  39. Khani S, Farmani A, Rezaei P (2023) Optical resistance switch for optical sensing. In: Momeni E, Jahed Armaghani D, Azizi A (eds) *Artificial Intelligence in Mechatronics and Civil Engineering*. Emerging Trends in Mechatronics. Springer, Singapore. [https://doi.org/10.1007/978-981-19-8790-8\\_1](https://doi.org/10.1007/978-981-19-8790-8_1)
  40. Fang H, Wei C, Wang D, Yuan L, Jiao S, Bao Z, Yang H (2020) Research on photonic crystal fiber based on a surface plasmon resonance sensor with segmented silver-titanium dioxide film. *J Opt Soc Am B* 37:736–744
  41. Lin Z, Jiang L, Wu L, Guo J, Dai X, Xiang Y, Fan D (2016) Tuning and sensitivity enhancement of surface plasmon resonance biosensor with graphene covered Au MoS<sub>2</sub>-Au films. *IEEE Photon J* 8(6):1–8
  42. Avsar A, Vera-Marun IJ, Tan JY et al (2015) Air-stable transport in graphene-contacted, fully encapsulated ultra-thin black phosphorus-based field-effect transistors. *ACS Nano* 9(4):4138–4145
  43. Bruna M, Borini S (2009) Optical constants of graphene layers in the visible range. *Appl Phys Lett* 94(3):03190
  44. Schreiber B, Wacinski C, Chiarello R (2013) Index of refraction as a quality control metric for liquids in pharmaceutical manufacturing. *Pharm Eng* 33(2):1–7
  45. Pal S, Prajapati YK, Saini JP (2020) Influence of graphene's chemical potential on SPR biosensor using ZnO for DNA hybridization. *Opt Rev* 27:57–64
  46. Hossain MB, Mehedi IM, Moznuzzaman M, Abdulrazak LF, Hossain MA (2019) High performance refractive index SPR sensor modeling employing graphene tri sheets. *Res Phys* 15:102719
  47. Srivastava A, Verma A, Das R, Prajapati YK (2020) A theoretical approach to improve the performance of SPR biosensor using MXene and black phosphorus. *Optik* 203:163430
  48. Mudgal N, Saharia A, Agarwal A, Ali J, Yupapin P, Singh G (2020) Modeling of highly sensitive surface plasmon resonance (SPR) sensor for urine glucose detection. *Opt Quantum Electron* 52(6):1–14

**Publisher's Note** Springer Nature remains neutral with regard to jurisdictional claims in published maps and institutional affiliations.

Springer Nature or its licensor (e.g. a society or other partner) holds exclusive rights to this article under a publishing agreement with the author(s) or other rightsholder(s); author self-archiving of the accepted manuscript version of this article is solely governed by the terms of such publishing agreement and applicable law.